Enhancing Signal Resolution in a Noisy Nonlinear Sensor

Alexander P. Nikitin, Nigel G. Stocks and Adi R. Bulsara

Abstract It is well known that the resolution (defined as the smallest change in the signal being detected or quantified) of a sensor can be improved by increasing the observation time T of the measurement; typically, the resolution scales as $1/T^a$. Typically $a = 0.5$, or $a < 0.5$ if low frequency noise is present. We show that a neuronal system can display an enhanced scaling in the resolution, with the parameter $a = 1$; this occurs when the "inter spike intervals" are negatively correlated. We also show that, by introducing negative correlations into the time domain response of a nonlinear dynamical sensor, it is possible to replicate this enhanced scaling. This affords us the possibility of designing a novel class of biomimetic sensors that results in improved signal resolution by functionally utilizing negative correlations.

1 Introduction

In any measurement, one aspires to the highest possible accuracy. If the accuracy of a single measurement is not acceptable, usually due to unacceptable measurement errors e.g. stemming from a noise-floor, than the measurements are repeated N times and a statistical average (usually just the arithmetic mean) of the measurable is computed. For statistically independent errors, the total error of the measure-

A. P. Nikitin (✉)
School of Engineering and School of Life Sciences, University of Warwick, Coventry CV4 7AL, UK
e-mail: a.nikitin@warwick.ac.uk

N. G. Stocks
School of Engineering, University of Warwick, Coventry CV4 7AL, UK
e-mail: n.g.stocks@warwick.ac.uk

A. R. Bulsara
Space and Naval Warfare Systems Center Pacific, Code 71000,
San Diego, CA 92152-6147, USA
e-mail: bulsara@spawar.navy.mil

V. In et al. (eds.), *International Conference on Theory and Application in Nonlinear Dynamics (ICAND 2012)*, Understanding Complex Systems,
DOI: 10.1007/978-3-319-02925-2_13,

ment is reduced as $1/\sqrt{N}$, i.e. the accuracy of the measurement improves slowly in comparison to the rate of accumulation of the (statistical) data that are a part of the averaging operation. An improved scaling (improved rate of the reduction for measurement error with accumulating statistical data) is possible if the measurements are negatively correlated. This has been predicted to be a possibility in physiology [1]. Such living systems could, thus, improve their response to a weak target signal thereby benefitting from neagative correlations.

It is, of course, a very attractive undertaking to design engineering systems (or sensors) as analogs of a biological system which has (qualitative) matching dynamics. This is the aim of this paper. We show how the configuration and operation of a candidate nonlinear sensor having a temporal (in this case, event-based) readout, can be adapted to mimic the dynamics of an integrate-fire neuron with negatively correlated inter-spike intervals; these ideas were formulated by us in recent work [2]. We show that the sensor in this "biomimetic" mode yields a greatly reduced measurement error with the improved scaling $1/N$, when certain constraints (that will be quantified) are met.

In what follows, we start with the simplest neural dynamical model (perfect integrate-fire) and use it to explain the concept of "negative correlations"; we also introduce a definition of the neuron's resolution. The rest of the paper is concerned with a simple nonlinear dynamic sensor, a single-core fluxgate magnetometer, that operates in the time domain and whose dynamics can be mapped to the (integrate-fire) neural dynamics. Operating the magnetometer in this "biomimetic mode" is shown to lead to improved magnetic signal detection.

2 Perfect Integrate-Fire (PIF) Neuron Model

It has been shown [1] that electrosensory afferents of weakly electric fish have non-renewal statistics characterized by the fourth (or higher) Markov order. This means that a minimally correct model of neuronal spike trains for the electrosensory afferents should comprise four stochastic equations. It was also shown [1], that the observed significant improvement in the detectability of a weak signal by the electrosensory afferents, can be accounted for by a model of Markov order one. Such first Markov order models as the Perfect Integrate Fire (PIF) model with noisy threshold [3] are, in fact, known to describe a noise canceling mechanism that might, in fact, be realized in real neurons. We will see, later in this work, that the simple PIF model affords a prototype of the biomimetic magnetic field sensor. First, however, we discuss the effects of negative correlations in a simple PIF model.

The PIF model with noisy threshold can be described by the following equation,

$$\dot{v} = \beta + s, \tag{1}$$

where s is the (constant) signal to be estimated, β a constant bias current, and v the voltage across the nerve membrane. The threshold θ is a uniformly distributed

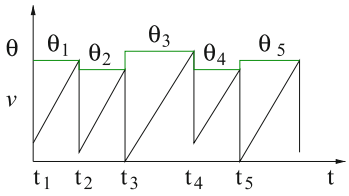

Fig. 1 The PIF model: dynamics of the membrane voltage v and the threshold θ

random variable, $\theta \in [\theta_a - D_u, \theta_a + D_u]$, that is independently defined for every inter-spike interval. D_u is the noise intensity, and θ_a the mean threshold, $\theta_a = \langle\theta\rangle$. The mode of operation is as follows: when the voltage v reaches the threshold θ, a spike is fired, a new threshold is chosen, and the voltage is reset to a new level $\eta = \theta - \theta_a$; this is schematized in Fig. 1. The ISIs generated by the model (1), with the above configuration of the threshold following each firing event, are strongly negatively correlated.

Denoting the times at which the level crossings occur as $t_0, t_1, \ldots, t_k$, the values of the threshold at crossing as $\theta_0, \theta_1, \ldots, \theta_k$, and the reset levels as $\eta_0 = \theta_0 - \theta_a, \ldots, \eta_k = \theta_k - \theta_a$ it is straightforward to show from (1) that the kth interspike interval (ISI) is given by,

$$T_k = (t_k - t_{k-1}) = \frac{\theta_k - \theta_{k-1} + \theta_a}{\beta + s}. \tag{2}$$

We decompose the inter-spike interval T_k into three quantities so that

$$T_k = \delta_k + \Delta - \delta_{k-1},$$

where we introduce the "jitters" δ_{k-1} and δ_k as

$$\delta_k = \theta_k/(\beta + s), \qquad \delta_{k-1} = \theta_{k-1}/(\beta + s),$$

and the mean inter-spike interval,

$$\Delta = \langle T_k\rangle = \theta_a/(\beta + s). \tag{3}$$

If the threshold is noiseless, and the signal $s = const$, then the process is exactly periodic because the spikes occur, precisely, at times $t_k = k\Delta + t_0$.

The serial correlation coefficient of the stochastic process can be calculated as,

$$\rho(m) = \frac{\langle (T_k - \langle T_k\rangle)(T_{k+m} - \langle T_{k+m}\rangle)\rangle}{\sigma_{T_k}\sigma_{T_{k+m}}} = \begin{cases} 1 : m = 0, \\ -\frac{1}{2} : m = 1, \\ 0 : m > 1. \end{cases} \tag{4}$$

It is easy to see the ISIs generated by the model (1) are strongly negatively correlated with $\rho(1) = -0.5$.

We now introduce the sum of N inter-spike intervals,

$$\tau_{ob,N} = \sum_{k=1}^{N} T_k = \delta_N - \delta_0 + N\Delta, \tag{5}$$

which is equivalent to an observation time in the measurement. The average of this sum is the mean observation time

$$T_{ob} = \langle \tau_{ob,N} \rangle = N\Delta, \tag{6}$$

and the variance,

$$\sigma^2_{\tau_{ob,N}} = 2\sigma^2_{\delta}, \tag{7}$$

is independent of N. This means that the noise in our measurement does not accumulate with an increasing number (N) of measurements. This is a direct result of the noise canceling mechanism that makes it attractive for practical applications to engineered systems .

To characterize the accuracy of the signal s estimation from the ISIs, we introduce the resolution R defined in [2, 4] as,

$$R = \left| \frac{\partial T_{ob,N}}{\partial s} \right|^{-1} \sigma_{\tau_{ob,N}}, \tag{8}$$

R is the smallest resolvable value of the measured quantity. The resolution is readily derived via a Taylor expansion of T_{ob} about $s = 0$: $T_{ob}(\delta s) = T_{ob}(0) + dT_{ob}/ds \times \delta s$. Noting that, physically, the resolution represents the signal value that results in $\sigma_{\tau_{ob,N}}$ being equal to the difference in T_{ob} with and without signal, we see that the resolution is given by $dT_{ob}/ds \times \delta s$ where the differential is evaluated at $s = 0$. Finally we set $\delta s = R$ when $\sigma_{\tau_{ob,N}} = T_{ob}(0) - T_{ob}(s)$. One can readily obtain the resolution R for the PIF model in the limit of very small target signal as:

$$R = \left| \frac{\partial}{\partial s} \frac{N\theta_a}{\beta + s} \right|^{-1}_{s=0} \sqrt{2}\sigma_{\delta} = \frac{\sqrt{2}\sigma_{\delta}\beta^2}{\theta_a} \frac{1}{N}, \tag{9}$$

which is seen to be proportional to $1/N$, an improvement over the $1/\sqrt{N}$ dependence for typical renewal processes (without negative correlations). We remind the reader that a smaller value for R implies better signal detection/quantification performance.

3 A Magnetic Field Sensor in the Biomimetic Mode

The PIF model, introduced above, can be characterized by (i) the dependence (i.e. rise) of the membrane voltage with external signal, and (ii) a comparator which imposes the threshold which, in turn, triggers (iii) the resetting mechanism. To operate in the "biomimetic mode", a sensor should mimic the oscillatory dynamics of the PIF model with negative correlations in its inter-spike intervals to exploit the noise canceling mechanism. We now consider the dynamics of a fluxgate magnetometer [4] that is operated in the temporal domain.

It is well known that the relaxation time of the magnetization variable in a ferromagnetic core depends on an applied external magnetic field. By altering the directions of the applied magnetic field, we can generate conditions for the ferromagnet under which its magnetization will periodically increase and decrease, i.e. it will oscillate (the oscillations are non-sinusoidal, of course). We can map the ferromagnetic core dynamics onto a PIF neuronal model by associating the increasing magnetization with the increasing membrane voltage of the cell membrane, and the decreasing magnetization with the reset in the membrane voltage.

As might be imagined, some engineering problems must be solved for a practical realization of the biomimetic mechanism. First, the magnetization is an internal parameter of the ferromagnet, and it is not easy to measure it directly. Therefore we replace, in our measurements, the magnetization with the B-field that is a linear combination of an unknown field B_0 (the target field that is to be measured), the known field B_+ that is used to induce the relaxation dynamics, and the magnetization M:

$$B = B_0 + B_+ + \mu_0 M, \tag{10}$$

where μ_0 is the magnetic constant. Since B_0 and B_+ are assumed to be constants during the relaxation process, the B field relaxes like the magnetization with rate

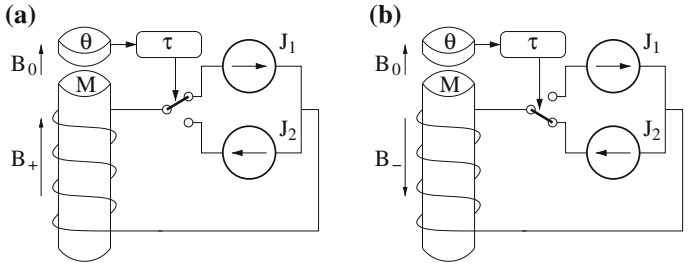

Fig. 2 The magnetic field sensor. **a** The magnetization M increases in the presence of the magnetic fields B_+ and B_0. The field B_+ is assumed to be $B_+ \gg |B_0|$ and corresponds to the current J_1 in the coil. **b** The resetting of the core magnetization occurs when the it reaches a threshold value θ in the magnetic comparator. At this point, the current J_1, in the coil, is replaced by the current J_2 for a time interval τ; this corresponds to a magnetic field switch from B_+ to B_- with an attendant coil current J_2

$dB/dt = \mu_0 dM/dt$. Having made the change in variables, we can use any B field sensor, with a very sharp sigmoidal characteristic, as a comparator of the B field with a threshold θ that will trigger the reset mechanism (see Fig. 2). The second engineering problem stems from the impossibility of, instantly, resetting the magnetization M in the ferromagnet. To reset the magnetization, we need to replace the magnetic field B_+ with B_- and this field is applied for a duration τ, to allow the magnetization to reach an acceptable level (this level is a 'design parameter' that is controlled via τ – careful selection is required for optimal performance); this is schematized in Fig. 2b.

The dynamics of the magnetization M of a single–domain ferromagnetic core in the one dimensional case can be described by the following differential Eq. (5) (see [4]),

$$\tau_a \frac{dM}{dt} = -M + M_s \tanh\left(\frac{CB}{\mu_0}\right), \tag{11}$$

where M_s is the saturation level of the magnetization, and τ_a its characteristic relaxation time. In Eq. (11), C is a non-linearity parameter that is proportional to the Curie temperature-to-temperature ratio. The parameter C characterizes the 'ferromagnet–paramagnet' phase transition: if $C > 1$ the core remains in its ferromagnetic phase; if $C < 1$ the core is in the paramagnetic phase. We now consider the magnetization in two operating scenarios.

3.1 The Noiseless Case

In the noiseless case, the magnetic sensor mimics a periodic oscillator. The phase plane of this oscillator is plotted in Fig. 3 wherein we show a working region of the parameters M and B bounded by the sections (branches) EF and GH. All the nonlinear dynamics occur on these branches. Switches between the branches occur

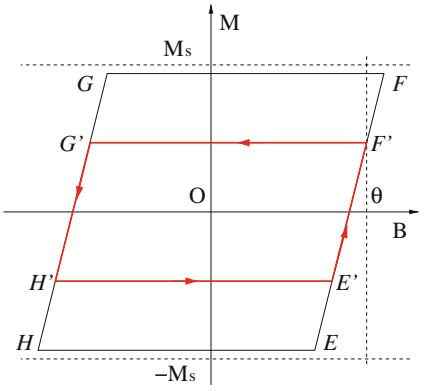

Fig. 3 The phase plane of the ferromagnetic oscillator in the variables M and B. The "limit cycle" $E'F'G'H'$ is shown in *red* with the *arrows* indicating the direction of motion on the phase plane. *Dashed lines* show the saturation levels $-M_s$ and M_s of the ferromagnet, and the threshold level θ

in two cases: when the B field crosses the threshold level θ; and when the system is forced to the branch GH for a duration τ.

The points in Fig. 3 have the following coordinates:

$$\begin{aligned} E &= \left[B_0 + B_+ + \mu_0 M_H, \quad M_H\right], \\ F &= \left[B_0 + B_+ + \mu_0 M_F, \quad M_F\right], \\ G &= \left[B_0 + B_- + \mu_0 M_F, \quad M_F\right], \\ H &= \left[B_0 + B_- + \mu_0 M_H, \quad M_H\right], \end{aligned} \tag{12}$$

where the parameters M_H and M_F can be found from the equation $dM/dt = 0$. This condition leads to the transcendental equations:

$$M_H = M_s \tanh\left(C\frac{B_0 + B_-}{\mu_0} + CM_H\right),$$

$$M_F = M_s \tanh\left(C\frac{B_0 + B_+}{\mu_0} + CM_F\right),$$

whose solutions M_H and M_F can be found numerically (here we assume that $-M_s < M_H < M_F < M_s$). We observe that the working region is less than the physically permitted states $[B, M]$ of the oscillator. The true region of acceptable values for the magnetization would, normally, be bounded by the saturation values $-M_s$ and M_s instead of M_H and M_F. However, we are concerned with the working region of the phase plane that is acceptable for the periodic oscillations, i.e. the region where an attractor can be located.

The role of a limit cycle (attractor) is played by the quadrilateral $E'F'G'H'$. Suppose a trajectory of the dynamical system starts at E' where, according to the equation $B = B_0 + B_+ + \mu_0 M$, the magnetization M is linearly dependent on the B field. Both M and B are non-linearly growing quantities due to Eq. (11). As the B field crosses the threshold θ (point F'), the trajectory is instantly switched to the point G'. Now the trajectory, according to Eq. (11), relaxes during the time interval τ to the point H'. Then, the trajectory instantly switches onto the branch EF (the point E'). It is easy to see from Fig. 3 that, for the existence of periodic oscillations, the threshold θ should satisfy the condition,

$$B_0 + B_+ + \mu_0 M_H < \theta < B_0 + B_+ + \mu_0 M_F.$$

If $\theta > B_0 + B_+ + \mu_0 M_F$ (the vertical dashed line does not cross the branch EF), then F is a stable point. We note that we are using a discrete two-state dynamical characterization i.e. for simplicity, we are using the instantaneous switches and the resetting time τ instead of a system of differential equations and their solutions. This means that a bifurcation (likely of saddle-node type) occurs at $\theta = B_0 + B_+ + \mu_0 M_F$ but cannot be correctly characterized unless we use the full differential equations to characterize the dynamical behavior (i.e. switching events and the resetting mecha-

nism). The above treatment (assuming the device to behave like a static nonlinearity) is valid as long as the characteristic time constant τ_a is the smallest time-scale in the system.

3.2 The Threshold Noise Case

Analogous with [3] we introduce noise in the threshold θ as a uniformly distributed variable in the interval $[\theta_a - D_u : \theta_a + D_u]$. According to our analysis of the magnetic sensor model in Sect. 3.1, the sensor output will retain its oscillatory properties if the parameters of the threshold noise satisfy the following inequalities, $\theta_a - D_u > M_H$ and $\theta_a + D_u < M_F$. It is important to note that, for modeling purposes, all noise sources are assumed to be internal to the sensor (the resolution is an intrinsic property of the sensor and cannot be defined in the presence of external noise); these are

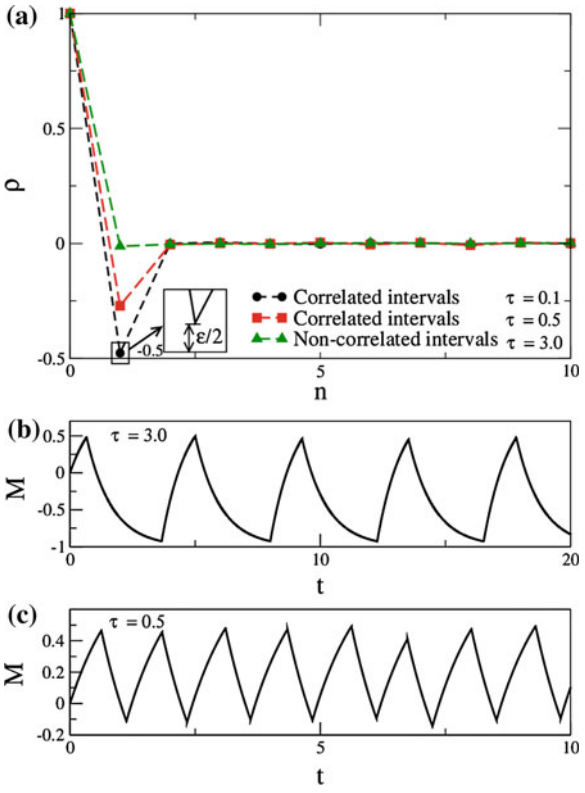

Fig. 4 **a** The correlation coefficient $\rho(n)$. **b** and **c** The magnetization M as a function of time t for the model described via (11). The time series corresponds to non-correlated intervals in **b** ($\tau = 3.0$) and negatively correlated intervals in **c** ($\tau = 0.5$). The parameters are $\theta_a = 2.5,\ D_u = 0.05,\ \mu_0 = 1,\ B_+ = -B_- = 2,\ C = 3$, and $B_0 = 0$

"consolidated" into an effective threshold noise. In our experiments (see e.g. [4] and references therein) we find that this is, in fact, a good assumption; the switching events are relatively clean with sensor noise appearing as a flucuating threshold.

Numerical simulations of Eq. (11) show that the level that the magnetization is reset to is strongly dependent on τ. For large τ (see Fig. 4b for $\tau = 3$) the magnetization approaches the saturation value and this reduces the negative correlation, as observed in the behavior of $\rho(1)$ (see Fig. 4a for $\tau = 3.0$). The reduction in negative correlation occurs because saturation of the magnetization results in a loss of memory in the magnetization variable when the threshold is crossed; for very strong saturation the magnetization is, effectively, reset to the same value every time with all memory effects being removed. In the opposite case, when τ is small, the level that the magnetization is reset to strongly depends on the value of the magnetization when the threshold was crossed and, hence, strong negative correlation is observed (see Fig. 4c for $\tau = 0.5$). The negative correlations can be characterized by the parameter ε, introduced as the half distance to $-1/2$ (see Fig. 4a),

$$\rho(1) = -\frac{1}{2} + \frac{\varepsilon}{2}.$$

The target magnetic field B_0 can be estimated from N time intervals, T_i, $i = 1, 2, ..., N$ as the total observation time $\tau_{ob} = \sum_{i=1}^{N} T_i$. The resolution, R, of the magnetic sensor is, then, defined via Eq. (8) with the replacement

$$\sigma_{\tau_{ob,N}} = \sigma_{\tau_{ob}} = \sqrt{\langle [\tau_{ob} - T_{ob}]^2 \rangle},$$

with the mean observation time identified as $T_{ob} = \langle \tau_{ob} \rangle$, and $s = B_0$ the target signal.

The (monotonic) dependence of the observation time T_{ob} on the external magnetic field B_0 is shown in Fig. 5a. This dependence can be used to estimate the target field. Fig. 5b shows that the resolution, R, has the scaling $T_{ob}^{-0.5}$ for the non-correlated intervals (e.g. for parameter value $\tau = 3.0$). However, when strong negative correlations exist (e.g. $\tau = 0.1$) the scaling is more complex. The scalings T_{ob}^{-1} and $T_{ob}^{-0.5}$ are shown as the black and red straight lines and these are seen to asymptote to the $\tau = 0.1$ data at small and large observation times respectively. This provides clear evidence that, at short observation times, the enhanced scaling T_{ob}^{-1} is observed; this scaling crosses over to $T_{ob}^{-0.5}$ at large observation time.

We have obtained theoretical results [6] that show that this dual scaling behavior appears to be a universal property in the sense that it occurs for linear and nonlinear reset mechanisms and in models of sensors and neural models. Moreover, our theory predicts the number of periods N^* at which the scaling crosses over from T_{ob}^{-1} to $T_{ob}^{-0.5}$; the result is $N^* \simeq 1/\varepsilon$ (see Fig. 5b) (note that the parameter ε can be estimated directly from the numerical results presented in Fig. 4a).

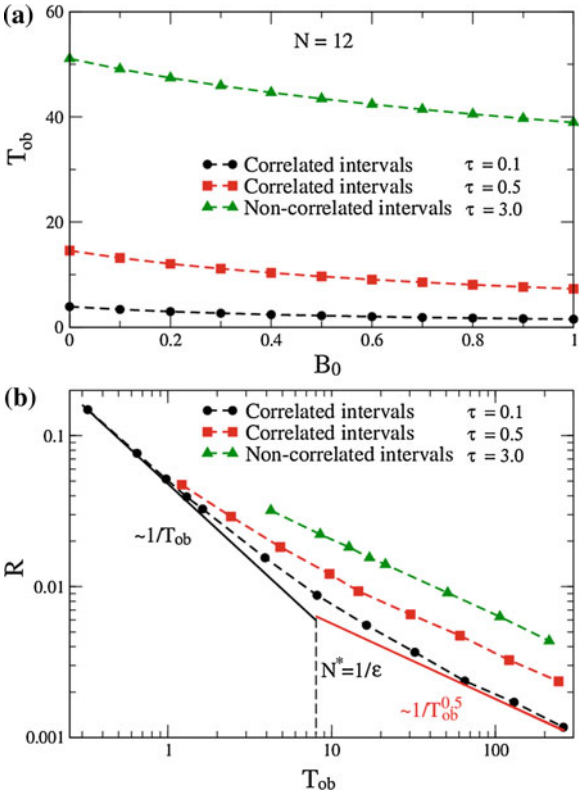

Fig. 5 **a** The observation time T_{ob} as a function of the external magnetic field B_0. **b** The resolution, R, versus the observation time, T_{ob}. The parameters are $\theta_a = 2.5$, $D_u = 0.05$, $\mu_0 = 1$, $B_+ = -B_- = 2$, $C = 3$

4 PIF Model with Deterministic Errors in the Reset

To explain the double scaling in the magnetometer model (see previous section), we introduce here the following solvable model with "deterministic errors" in the reset. The model is a modified PIF model (MPIF); it differs from the standard PIF model only through the different reset mechanism. In the PIF model, the resetting levels are $\eta_k = \theta_k - \theta_a$, i.e. the resetting level η_k is the result of a precisely shifted threshold θ_k. In the MPIF model, the shift of the threshold θ_k occurs with a "distortion" due to the transformation,

$$\eta_k = (\theta_k - \theta_a)(1 - c).$$

In Fig. 6, it is easy to see that the function $\eta(t)$ reproduces the dynamics of $\theta(t)$ with a compression on the v-axis. Thus, the parameter c is called the "compression". If $c = 0$, the MPIF model coincides with the PIF model; for $c = 1$, the resetting occurs

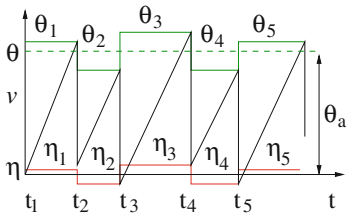

Fig. 6 Modified PIF (MPIF) model: typical dynamics of the membrane voltage v, the threshold θ and the resetting level η

at the constant level, $\eta_k = 0$. In this case, it should produce renewal oscillations. Hence, the compression c plays a role similar to the parameter τ in the magnetometer model.

Since the kth inter-spike interval produced by the MPIF model is

$$T_k = (t_k - t_{k-1}) = \frac{\theta_k - \theta_{k-1} + (1-c)\theta_a + c\theta_k}{\beta + s}, \tag{13}$$

we can decompose it into three random variables so that

$$T_k = \delta_k + \Delta_k - \delta_{k-1},$$

where we introduce the "jitter" terms $\delta_k = \theta_k/(\beta + s)$, $\delta_{k-1} = \theta_{k-1}/(\beta + s)$, and the noisy component of the ISI

$$\Delta_k = \frac{\theta_a}{\beta + s} + c\frac{\theta_{k-1} - \theta_a}{\beta + s}. \tag{14}$$

The variable Δ_k in Eq. (14) differs from Δ in Eq. (3) through a noisy component that is proportional to the parameter c. Therefore, the sum of N time intervals

$$\tau_{ob,N} = \sum_{k=1}^{N} T_k = \delta_N - \delta_0 + N\frac{\theta_a}{\beta + s} + \frac{c}{\beta + s}\sum_{k=0}^{N-1}(\theta_k - \theta_a) \tag{15}$$

includes the noisy term that is proportional to c and increasing with N.

The serial correlation coefficient differs from the one calculated for the PIF model; it has the additional term,

$$\rho(1) = -\frac{1}{2} + \frac{\varepsilon}{2}, \tag{16}$$

where the parameter ε is introduced as

$$\varepsilon = \frac{c^2}{2(1-c) + c^2}. \tag{17}$$

For very weak compression, $c \ll 1$, the last equation reduces to

$$\varepsilon \simeq \frac{c^2}{2}. \tag{18}$$

It is easy to show that the average observation times for both the PIF and the MPIF models are identical, $T_{ob} = \langle \tau_{ob,N} \rangle = N\theta_a/(\beta + s)$, but the variances are different. Moreover, in contrast to Eq. (7), the variance for the MPIF model,

$$\sigma^2_{\tau_{ob,N}} = 2\sigma^2_\delta \left(1 + c + N\frac{c^2}{2}\right), \tag{19}$$

increases with N. This dependence on N influences the resolution R. The resolution R for the MPIF model in the limit of an infinitesmially small target signal is

$$R = \frac{\sqrt{2}\sigma_\delta \beta^2}{\theta_a} \frac{1}{N} \sqrt{1 + c + N\frac{c^2}{2}}, \tag{20}$$

which, for a very weak compression $c \ll 1$, and using the approximation Eq. (18) becomes

$$R = \frac{\sqrt{2}\sigma_\delta \beta^2}{\theta_a} \frac{1}{N} \sqrt{1 + \varepsilon N}. \tag{21}$$

Now, it is easy to see that the resolution R has different scaling for different ranges of N. If $N \ll 1/\varepsilon$, the resolution is

$$R \simeq \frac{\sqrt{2}\sigma_\delta \beta^2}{\theta_a} \frac{1}{N};$$

If $N \gg 1/\varepsilon$, the resolution is

$$R \simeq \frac{c\sigma_\delta \beta^2}{\theta_a} \frac{1}{\sqrt{N}}.$$

Since the observation time T_{ob} is proportional to N, the resolution also has the double scaling in the terms of the observation times, $1/T_{ob}$ and $1/\sqrt{T_{ob}}$.

5 Conclusion

We conclude that operating a nonlinear sensor in the biomimetic mode can improve its performance, as quantified via the resolution. In particular, the analysis indicates that, absent the luxury of a long observation time, the above mode of operation might be particularly helpful. We reiterate that there is nothing special about the single core fluxgate magnetometer (used, here, as a test device); operating a generic nonlinear sensor in the correct working range should allow the benefits of negative correlations to be realized.

Acknowledgments The authors gratefully acknowledge support from the US Office of Naval Research and the US Office of Naval Research-Global.

References

1. R. Ratnam, M. Nelson, J. Neurosci. **20**(17), 6672–6683 (2000)
2. A. P. Nikitin, N. G. Stocks, A. R. Bulsara, Phys. Rev. Lett. **109**, 238103 (2012)
3. M. J. Chacron, B. Lindner, A. Longtin, Phys. Rev. Lett. **92**, 080601 (2004)
4. S. Baglio et al., IEEE Trans. Instr. Meas. **60**, 667 (2011)
5. H. E. Stanley, Introduction to Phase Transitions and Critical Phenomena (Oxford University Press, Oxford, 1971)
6. A. P. Nikitin, N. G. Stocks, A. R. Bulsara (to be published)